

Amplification in the auditory periphery: the effect of coupling tuning mechanisms

K.A. Montgomery

Mathematics Department, University of Utah, Salt Lake City, UT 84112

M. Silber

Department of Engineering Sciences & Applied Mathematics, Northwestern University, Evanston, IL 60208

S.A. Solla

Departments of Physics & Astronomy and Physiology, Northwestern University, Evanston, IL 60208

(Dated: June 19, 2017)

A mathematical model describing the coupling between two independent amplification mechanisms in auditory hair cells is proposed and analyzed. Hair cells are cells in the inner ear responsible for translating sound-induced mechanical stimuli into an electrical signal that can then be recorded by the auditory nerve. In nonmammals, two separate mechanisms have been postulated to contribute to the amplification and tuning properties of the hair cells. Models of each of these mechanisms have been shown to be poised near a Hopf bifurcation. Through a weakly nonlinear analysis that assumes weak periodic forcing, weak damping, and weak coupling, the physiologically-based models of the two mechanisms are reduced to a system of two coupled amplitude equations describing the resonant response. The predictions that follow from an analysis of the reduced equations, as well as performance benefits due to the coupling of the two mechanisms, are discussed and compared with published experimental auditory nerve data.

PACS numbers: 02.30.Oz, 87.16.Xa, 87.19.Bb

I. INTRODUCTION

The natural environment presents the auditory system with the challenge of responding to sounds over many orders of magnitude; the threshold of hearing and the threshold of pain differ by about thirteen orders of magnitude. For the ear to discriminate between sounds over such a large dynamic range, it is necessary for auditory stimuli to be compressed into a much smaller, more achievable range of physical responses. This is accomplished through a nonlinear mechanism in which small amplitude sounds are amplified to a greater extent than larger amplitude sounds. In order to process complex sound stimuli, it is also necessary for the auditory system to distinguish between the frequency components of the stimuli. The ear's amplification and frequency discrimination properties are thought to be derived from a common, metabolically-powered mechanism, the details of which have been the topic of much investigation [1, 2, 3].

In both mammals and nonmammals, hair cells of the inner ear are responsible for translating sound-induced mechanical stimuli into a neurotransmitter signal which induces the firing of the auditory nerve [4, 5]. Each hair cell consists of a cell body which is contacted from below by the auditory nerve and a hair bundle consisting of actin-supported fibers. When sound stimulates the auditory organ, the resulting motion of the hair bundle causes transduction channels to be mechanically pulled open. Ionic current then enters the cell body through the transduction channels, thereby depolarizing the cell, and ultimately causing the release of neurotransmitter at the auditory nerve synapse.

In mammals, the frequency-discrimination properties of the basilar membrane, the membrane in which the hair cells are embedded, contribute to the auditory system's capacity to distinguish between sounds of different frequencies. By contrast in nonmammals, the surface in which the hair cells are embedded lacks tuning properties. The nonmammalian auditory system is thought to achieve its frequency tuning properties through two different mechanisms, both intrinsic to the hair cell. The first mechanism involves the mechanical motion of the hair bundle. Experiments indicate that the hair bundle responds actively, with greater energy than provided by the stimulus, if forced near its resonance frequency [6]. Evidence for a second mechanism, referred to as electrical resonance, is provided by the decaying oscillations that are observed in the membrane potential of the cell body in response to constant current injection [7]. These oscillations indicate that the cell body possesses a preferred response frequency.

Dynamical systems methods have proven useful in analyzing the frequency tuning and amplification properties of physiologically-based auditory models. Interestingly, models of both the active motion of the hair bundle and the electrical resonance mechanism have been shown to be poised near a Hopf bifurcation [8, 9]. A Hopf bifurcation is a robust mechanism for generating spontaneous oscillations as a control parameter of a nonlinear system is varied. It occurs when a static equilibrium loses stability via a complex conjugate pair of eigenvalues (of the associated linear stability problem) crossing the imaginary axis in the complex plane with nonzero imaginary part. It has been

suggested that the hair cell critically tunes itself so that its parameters are poised just below the bifurcation point, thereby making the cell sensitive to stimuli at the Hopf bifurcation frequency, without causing spontaneous oscillations [10, 11]. These investigations determine the generic frequency tuning and amplification properties of a periodically-forced system in the vicinity of a Hopf bifurcation; specifically, they analyze the characteristics of solutions that are frequency-locked to a weak, additive resonant forcing term. Sufficiently close to the Hopf bifurcation point, the system is compressively nonlinear: small inputs are amplified to a greater extent than larger ones [10, 11]. Moreover, the compression of the dynamic range is accompanied by frequency tuning, which is sharper for small amplitude inputs than for larger amplitude signals.

Previous studies of hair cell amplification models have considered the normal form for a system near a Hopf bifurcation without actually performing the normal form reduction from the physiologically relevant mathematical model. Here, in Appendix II, we reduce the Hudspeth and Lewis model of the electrical tuning mechanism [12, 13] to the normal form for a system near a Hopf bifurcation, thereby determining the numerical values of the coefficients of the normal form corresponding to the model and parameters used by Hudspeth and Lewis. We find that the coefficient of the nonlinear term in the normal form has comparable real and imaginary parts; it is not purely real as was assumed in earlier investigations [10, 11]. We show that a result of the nonzero imaginary part is that the response of the system to resonant forcing may be hysteretic and that the frequency tuning curves are no longer symmetric about the resonance frequency. We further propose a model that describes weak coupling between the hair bundle amplification mechanism and the electrical resonance mechanism. We assume that both oscillation mechanisms are critically tuned to approximately the same resonant frequency and only weakly damped so that the Hopf bifurcation normal form applies to each independently, *i.e.* when the other mechanism is suppressed. We then assume weak linear coupling of the mechanisms, and direct forcing of the hair bundle at a frequency that is close to its natural frequency. As in earlier investigations, the analysis focuses on the frequency-locked solutions, and, in particular, on how the magnitude of response grows with the forcing. We find that the combined critically-tuned amplification system, can lead to a response, R , that scales with $F^{1/9}$, where F is the resonant forcing amplitude, thereby leading to enhanced amplification, R/F , of small signals. We also explore the enhanced frequency-tuning characteristics of the combined mechanical and electrical amplification system, comparing it with those associated with a single tuning mechanism.

Our paper is organized as follows. In section II we introduce the reduced mathematical model, with the mathematical details of the reduction from the physiologically-detailed models relegated to Appendix II. Section III contains our analysis of the reduced model, focusing particularly on the simpler situation of unidirectional coupling from the hair bundle tuning mechanism to the electrical resonator. We present response-versus-forcing curves that demonstrate the transition from a linear response ($R \propto F$) to a response $R \propto F^{1/9}$ as the amplitude of the (weak) signal increases. We also demonstrate the sharper tuning that is possible with the combined amplification system. Finally, section IV compares our model predictions with published experimental auditory nerve data.

II. MODEL

Two distinct mechanisms contribute to auditory tuning in nonmammalian vertebrates: an ‘electrical’ resonance arising from an interplay between ionic currents through the cell membrane, and a ‘mechanical’ resonance associated with the active motion of the stereocilia in response to stimuli at their resonance frequency. We start our discussion by focusing on the electrical resonance mechanism. The underlying biophysical components have been discussed by Hudspeth and Lewis [12, 13], who performed a set of experiments that carefully characterized the dynamical properties of the major ion channels on the cell bodies of bullfrog saccular hair cells. On the basis of these experiments, they developed a single compartment model of the hair cell (see Appendix I) using the simplifying assumption that only two major active ion channels, a voltage-gated calcium channel and a calcium-gated potassium channel, contribute to the cell’s dynamical behavior. In this model, the dynamical evolution of the membrane potential V_m is given by an equation based on the direct application of Kirchoff’s laws to a circuit that represents the flow of ions across the membrane:

$$-C_m \frac{dV_m}{dt} = g_{Ca} m^3 (V_m - E_{Ca}) + g_{K(Ca)} (O_2 + O_3) (V_m - E_K) + g_L (V_m - E_L) - I. \quad (1)$$

Here V_m is the membrane potential and C_m is the membrane capacitance per unit area. The voltage-gated calcium (Ca) current is represented by $g_{Ca} m^3 (V_m - E_{Ca})$, where g_{Ca} is the maximum Ca conductance per unit area, m is the voltage-dependent fraction of open conformational subunits in the Ca channels, and E_{Ca} is the reversal potential for the Ca ion channels. The Ca-gated potassium (K) current is represented by $g_{K(Ca)} (O_2 + O_3) (V_m - E_K)$, where $g_{K(Ca)}$ is the maximum K conductance per unit area, $(O_2 + O_3)$ is the fraction of K channels in one of their two open states, and E_K is the reversal potential for the K ion channels. The term $g_L (V_m - E_L)$ represents all passive

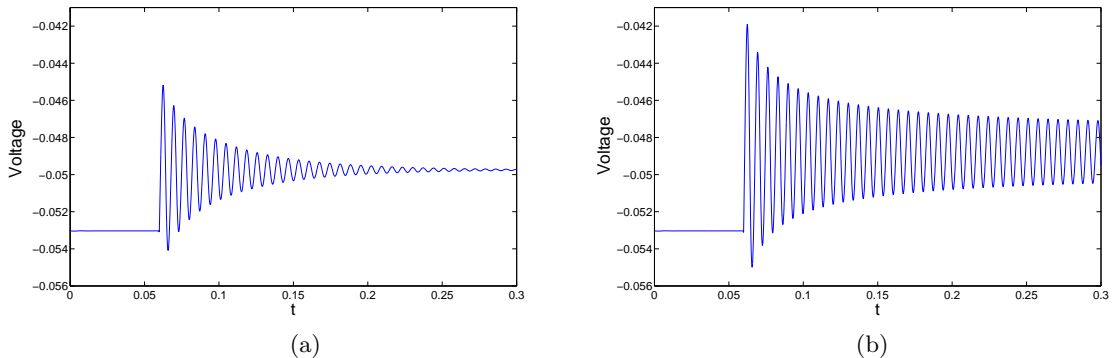


FIG. 1: Numerical simulations of the response of the membrane potential of a hair cell in the Hudspeth and Lewis model [12, 13], to a constant current, I , injected at $t = .06$. (a) $I = 65$ pA; (b) $I = 95$ pA. A Hopf bifurcation occurs at $I^* \approx 91.3$ pA. The other parameters of the H&L model (15), used in the simulations, are given in Appendix I.

ion channels as a leak conductance g_L per unit area and a reversal potential E_L . The command current I is directly injected into the cell body. The formulation of the model involves six additional equations (see Appendix I) that describe the dynamical evolution of the fraction m of open units in the Ca channels, the intracellular concentration of Ca ions close to the cell membrane, and the fraction of Ca-gated K channels in each of their three closed states (C_0, C_1, C_2) and two open states (O_2, O_3). In their seminal work [12, 13], Hudspeth and Lewis (H&L) experimentally characterized the value of the various parameters that appear in these equations.

The H&L model reproduces qualitatively the decaying membrane potential oscillations observed in current-clamp experiments in which a current of constant amplitude I is injected into the cell body [12, 13]. As shown in Figure 1, the response of the membrane potential to a step current of amplitude I depends crucially on the value of the injected current. For small injected currents, as illustrated in Figure 1(a), the membrane potential exhibits an oscillatory decay to a new constant value. For larger current values, as illustrated in Figure 1(b), the membrane potential decays to a new state that is oscillatory. This qualitative difference signals a transition between a regime in which the asymptotic state is a fixed point and a regime in which the asymptotic state is a limit cycle. In the H&L model, this transition occurs by a Hopf bifurcation [9].

A Hopf bifurcation occurs when a fixed point of a system of ODE's undergoes a change in stability in which a complex conjugate pair of eigenvalues $\lambda, \bar{\lambda}$ passes from the $Re(\lambda) < 0$ to the $Re(\lambda) > 0$ side of the imaginary axis in the complex plane. Figure 2 shows the evolution of the eigenvalues of the H&L model linearized around its fixed point, as the input current is increased from 0 and 100 pA. Note that three of the eigenvalues are always real and negative, and one complex conjugate pair remains in the $Re(\lambda) < 0$ semispace. The leading complex conjugate pair crosses the $Re(\lambda) = 0$ axis for $I^* \approx 91.3$ pA; this is the value of the input current at which the fixed point becomes unstable, as determined by fixing the parameters of the model at the experimentally-based estimates listed in Hudspeth and Lewis's original paper. That the H&L model is, for physiologically reasonable values of the parameters, poised near a Hopf bifurcation has profound implications for the signal processing capabilities of the modelled hair cell. Specifically, at the Hopf bifurcation the system is compressively nonlinear, as it exhibits a large amplification of small amplitude inputs and a smaller amplification of large amplitude inputs [10, 11]. Moreover, the resulting compression of the dynamic range is accompanied by a sharp frequency tuning of the response to small amplitude inputs and a broad tuning in the response to large amplitude inputs [10, 11].

The dynamical behavior of the model is asymptotically described by the amplitude of the mode associated with the most unstable eigenvector, which is the one associated with the complex conjugate pair of eigenvalues that cross the $Re(\lambda) = 0$ axis at the Hopf bifurcation. Sufficiently close to the bifurcation, the system can be generically described by a normal form equation [14]:

$$\frac{dA}{dt} = (a + ib)A + (c + id)|A|^2 A, \quad (2)$$

which characterizes the dynamical evolution of the complex amplitude A of the most unstable mode. In this equation, the parameter a is a measure of the distance to the Hopf bifurcation at $a = 0$; a is negative below the bifurcation and positive above. The parameter b is the frequency of the system at the bifurcation, and the parameter d measures the shift in preferred frequency as the amplitude of the solution increases, as readily seen by setting $A = re^{i\Omega t}$ in (2) to establish that $r = \sqrt{\frac{a}{-c}}$ and $\Omega = b + dr^2$. The parameter c distinguishes between supercritical ($c < 0$) and subcritical

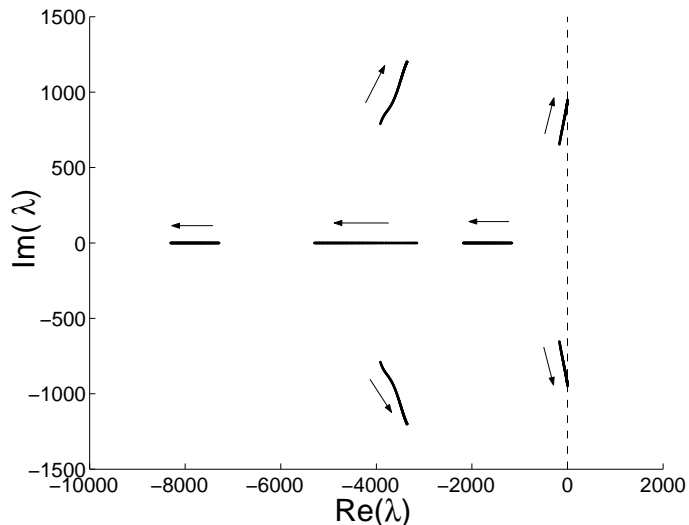


FIG. 2: The eigenvalues of the Hudspeth and Lewis model (15), linearized about its static equilibrium state as described in Appendix II, evolve in the complex plane as I is increased from 0 pA to 100 pA. Solid lines indicate the trajectory of the eigenvalues with increasing I . Other parameters of the equations are given in Appendix I.

($c > 0$) Hopf bifurcations.

We have carried out a standard nonlinear reduction of the H&L model to the normal form (see Appendix II). In the resulting normal form (26), a is proportional to $\Delta I = (I - I^*)/I^*$ and c is negative. This reduction thus establishes the supercritical nature of the Hopf bifurcation in the H&L model. For this supercritical bifurcation, there is a transition from a stable fixed point to a state in which the fixed point becomes unstable and a stable limit cycle exists. Moreover, in the supercritical case, the radius r of the limit cycle grows, with distance past the bifurcation point, with the characteristic scaling $r \propto \sqrt{\Delta I}$.

In the current-clamp experiments conducted by Hudspeth and Lewis [12, 13], the current injected into the cell was of constant amplitude. In contrast, natural inputs to the cell are due to a time-dependent, sound-induced mechanical displacement of the hair bundle, which results in time-dependent changes in the conductance through the transduction channels. Because the transduction channels are passive, this time-dependence can be incorporated into the H&L model through the leakage conductance term on the right-hand-side of (1). In the case of a simple time-periodic conductance, the reduction carried out in Appendix II suggests that for command currents close to I^* the most important contribution of the time-periodic forcing to the asymptotic dynamics comes from the Fourier component that is closest to the resonance frequency of the system. In the case of a weak periodic signal with frequency close to the resonator's frequency, the time-periodic input can be represented as an additive contribution to the amplitude equation, which then takes the form:

$$\frac{dA}{dt} = (a + ib)A + (c + id)|A|^2 A + Fe^{i\omega t}. \quad (3)$$

Due to the time-translation symmetry of the unforced case, we can, without loss of generality, assume that F is real and positive. We note that earlier investigations of (3) in the context of amplification mechanisms in auditory hair cells [10, 11] assumed a real coefficient of the nonlinear term, *i.e.* they made the nongeneric assumption that $d = 0$ such that the preferred frequency of the nonlinear oscillator had no amplitude-dependence.

We next consider the tuning mechanism associated with the mechanical deflection of the hair bundle. Experiments in which a glass fiber was attached to the hair bundle and used to mechanically stimulate the bundle at a specific frequency showed that the hair bundles respond preferentially to stimuli at their resonance frequency [6]. The motion of the hair bundles has been shown to be sensitive to the amount of calcium ion entering the transduction channels [15]. A model for hair bundle motion due to calcium binding within the stereocilia was proposed by Choe *et al.* [8]. In their model, when transduction current enters the hair bundle Ca ions attach themselves to the transduction channels at sites within the stereocilia; this attachment causes an increase in tension, which in turn causes the channel to close [8]. When the transduction channel closes, the Ca ions detach themselves from the binding sites and the channel returns to its regular tension allowing the cycle to repeat itself. Choe *et al.* have shown that, when the parameters of their model are specified within physiologically reasonable ranges, the model is near a Hopf bifurcation. Experimental evidence also indicates that the relationship between stimulus magnitude and magnitude of the hair bundle oscillations

obeys the scaling that would be expected for a system tuned near a Hopf bifurcation [16], lending support to our assumption that a model describing the hair bundle dynamics is poised near a Hopf bifurcation. Assuming this second mechanism is tuned sufficiently close to a Hopf bifurcation, it too can be reduced to the normal form (2) for a system near a Hopf bifurcation.

It only remains to consider first the manner in which the two tuning mechanisms are coupled in the biological system, and second how this coupling should be represented in the reduced model. One clear source of coupling between the two tuning mechanisms is through the transduction current. The magnitude of the transduction current entering through the stereocilia is directly related to the magnitude of displacement of the stereocilia. This relationship between displacement and the amount of current entering the cell has been measured indirectly by measuring the change in the receptor potential of the cell in response to stereocilia displacements of different magnitudes [17]. Such experiments indicate that, in absence of stimuli, a small amount of current is flowing into the cell through the stereocilia. When the hair bundle is deflected in the negative direction, away from the tallest stereocilia, transduction channels close and the amount of current flowing into the cell decreases. Similarly, when the hair bundle is deflected in the positive direction, the amount of current entering through the transduction channels increases and eventually saturates. For small displacements in the positive direction, the relationship between the displacement of the hair bundle and the change in the receptor potential is approximately linear [17]. As the amplitude of the hair bundle oscillations increases due to stimulation at the stereocilia's resonance frequency, the amount of current entering the cell body and providing a forcing to the second electrical resonance mechanism increases. This clearly provides a means of coupling from the stereocilia tuning mechanism to the electrical resonance mechanism.

There is also evidence for coupling in the reverse direction, from the electrical resonance mechanism to the hair bundle resonance mechanism, in that electrical stimulation of the cell body has been shown to induce displacement of the stereocilia [18, 19, 20, 21, 22]. The exact mechanism for coupling in this direction is less clear. Experimental comparisons between current injected into the cell body and the resulting displacement of the stereocilia indicate that the linear approximation is reasonable for small current injections [23]. The presence of coupling in both directions raises the question of whether there are actually two separate tuning mechanisms or the stereocilia tuning mechanism is simply a manifestation of the electrical tuning mechanism. This question was addressed in experiments in which the cell body was voltage clamped to silence electrical resonance oscillations allowing the motion of the stereocilia to be probed separately [24]. These experiments demonstrate active motion of the stereocilia even in the absence of the electrical resonance mechanism. Electrical resonance experiments are often performed by direct current injection, with transduction channels blocked, so the independence of the electrical resonance mechanism from the active motion of the stereocilia was never in question.

From the biological evidence, it is reasonable to assume that the coupling between the two mechanisms is linear for sufficiently small forcing. This leads us to a reduced model consisting of two coupled amplitude equations of the form,

$$\frac{dA_1}{dt} = (a_1 + ib_1)A_1 + (c_1 + id_1)|A_1|^2 A_1 + \gamma_1 e^{i\psi_1} A_2 + F e^{i\omega t}, \quad (4)$$

$$\frac{dA_2}{dt} = (a_2 + ib_2)A_2 + (c_2 + id_2)|A_2|^2 A_2 + \gamma_2 e^{i\psi_2} A_1. \quad (5)$$

In this model, (4) represents the hair bundle resonance mechanism which receives a sound-induced time-dependent forcing ($\propto F$) as well as feedback from the electrical resonance mechanism ($\propto A_2$). Equation (5) represents the electrical resonance mechanism which receives a forcing proportional to the displacement of the stereocilia. Note that we allowed for a phase difference ψ_j in each of the coupling terms, with the corresponding parameters γ_j taken to be real and non-negative. Moreover, we note that when both γ_1 and γ_2 are nonzero, then the Hopf bifurcations that cause spontaneous oscillations in the unforced problem ($F = 0$) will shift away from $a_j = 0$. As detailed mathematically in Appendix II, the model is valid for the case in which each system is tuned close to the Hopf bifurcation ($|a_j|$ sufficiently small), each system is tuned near the resonance frequency ($b_j \approx \omega$), and the forcing and the coupling are weak (F, γ_j sufficiently small).

We have determined from Hudspeth and Lewis's model the numerical values of the coefficients a_2, b_2, c_2, d_2 of (5) for H&L's physiological parameters. Models also exist for the stereocilia mechanism, so it is possible that the same coefficients of (4) could be determined based on these models. Performing the second reduction however would not be particularly useful in this paper because our analysis requires that both systems be tuned close to the same frequency. There are multiple ways to tune the physiological models such that they yield vibrations at a required frequency. Thus, without a very clear idea of the physiologically reasonable method to adjust the model parameters, there is no way to determine a consistent result for the numerical values of the coefficients in the amplitude equation (4).

Nonetheless, many of our conclusions regarding scaling laws hold provided that the Hopf bifurcations are supercritical (*i.e.* provided $c_j < 0$), and that our fundamental modeling assumptions are met.

III. ANALYSIS

A. Response-Versus-Forcing Relationship

Our analysis of the reduced model, Eqs. (4)-(5), focuses on frequency-locked solutions of the form $A_j = R_j e^{i(\omega t + \phi_j)}$, $j = 1, 2$, where $R_j \geq 0$ and $\phi_j \in [0, 2\pi)$ are constants. We wish to determine how the magnitude of the electrical response, measured by R_2 , scales with the sound-induced mechanical forcing amplitude F . This scaling depends on the proximity to the Hopf bifurcation, captured by the linear damping coefficients $a_j < 0$ in (4)-(5). It also depends on how closely tuned the natural frequencies, b_j , of the nonlinear oscillation mechanisms are to each other and to the driving frequency, ω .

Substituting $A_j = R_j e^{i(\omega t + \phi_j)}$ into (4)-(5) yields the following pair of complex-valued algebraic equations defining an implicit relationship between the real quantities F and R_2 :

$$F e^{-i\phi_1} = -(a_1 + i(b_1 - \omega))R_1 - (c_1 + id_1)R_1^3 - \gamma_1 R_2 e^{i(\phi_2 - \phi_1 + \psi_1)}, \quad (6)$$

$$\gamma_2 R_1 e^{i(\phi_1 - \phi_2 + \psi_2)} = -(a_2 + i(b_2 - \omega))R_2 - (c_2 + id_2)R_2^3. \quad (7)$$

We can solve (7) for R_1 in terms of R_2 :

$$R_1 = -\frac{e^{-i(\phi_1 - \phi_2 + \psi_2)}}{\gamma_2} \left((a_2 + i(b_2 - \omega))R_2 + (c_2 + id_2)R_2^3 \right). \quad (8)$$

Here we can determine the phase difference $(\phi_1 - \phi_2)$ by the requirement that R_1 be real and nonnegative. Substituting this expression into (6), we find

$$F = e^{i(\phi_2 - \psi_2)} \left(\alpha_1 R_2 + \alpha_3 R_2^3 + \alpha_5 R_2^5 + \alpha_7 R_2^7 + \alpha_9 R_2^9 \right), \quad (9)$$

where

$$\begin{aligned} \alpha_1 &\equiv -\gamma_1 e^{i(\psi_1 + \psi_2)} + \frac{1}{\gamma_2} (a_1 + i(b_1 - \omega))(a_2 + i(b_2 - \omega)), \\ \alpha_3 &\equiv \frac{1}{\gamma_2} (c_2 + id_2)(a_1 + i(b_1 - \omega)) + \frac{1}{\gamma_2^3} e^{-2i(\phi_1 - \phi_2 + \psi_2)} (c_1 + id_1)(a_2 + i(b_2 - \omega))^3, \\ \alpha_5 &\equiv \frac{3}{\gamma_2^3} e^{-2i(\phi_1 - \phi_2 + \psi_2)} (a_2 + i(b_2 - \omega))^2 (c_1 + id_1)(c_2 + id_2), \\ \alpha_7 &\equiv \frac{3}{\gamma_2^3} e^{-2i(\phi_1 - \phi_2 + \psi_2)} (a_2 + i(b_2 - \omega))(c_1 + id_1)(c_2 + id_2)^2, \\ \alpha_9 &\equiv \frac{1}{\gamma_2^3} e^{-2i(\phi_1 - \phi_2 + \psi_2)} (c_1 + id_1)(c_2 + id_2)^3. \end{aligned} \quad (10)$$

Again, the phase ϕ_2 in (9) is determined by the requirement that the forcing magnitude F be real and non-negative. It immediately follows from the polynomial form of (9) that the response R_2 need not be a single-valued function of F . It also follows that, with increasing forcing, there is a transition from a linear regime, $R_2 \propto F$, for sufficiently small forcing, to a regime where $R_2 \propto F^{1/9}$ for larger values of F . However, whether this transition occurs for small values of F , for which the model (4)-(5) is valid, depends on both the magnitude of the coupling coefficients γ_j and the magnitude of the linear coefficients $a_j + i(b_j - \omega)$. In particular, if we let $\epsilon = |a_2 + i(b_2 - \omega)|$, then we expect the transition to the regime $R_2 \propto F^{1/9}$ will occur for small F provided that $|a_1 + i(b_1 - \omega)|\gamma_2^2$ is at most $O(\epsilon^3)$, and $\gamma_1\gamma_2^3$ is at most $O(\epsilon^4)$.

The response *vs.* forcing characteristics associated with the model (4)-(5) are further explored in Fig. 3. For this figure, we assume supercritical Hopf bifurcations associated with the mechanical and electrical resonance mechanisms so that $c_j < 0$ in the model equations. With an appropriate re-scaling of amplitudes A_j , we may then assume $c_j = -1$ for both $j = 1$ and $j = 2$. Our direct calculation of the normal form coefficients in (5) (see Appendix II), from the H&L model, yields $d_2/c_2 \approx 1.1$. Thus in many of our numerical computations we set $d_2 = -1.1$. Finally, if we scale time by the dimensioned forcing frequency, we may take $\omega = 1$ in the model equations. Fig. 3 indicates stable frequency-locked

solutions as solid lines and unstable solutions by dotted lines. The linear stability of the frequency-locked solutions is determined by substituting the ansatz $A_j = R_j e^{i(\omega t + \phi_j)}(1 + z_j(t))$ into Eqs. (4)-(5) and then linearizing about $z_j = 0$. We then find that the perturbations z_j satisfy the following system of linear differential equations

$$\begin{pmatrix} \dot{z}_1 \\ \dot{\bar{z}}_1 \\ \dot{z}_2 \\ \dot{\bar{z}}_2 \end{pmatrix} = \begin{pmatrix} M_1 & M_2 & M_3 & 0 \\ \bar{M}_2 & \bar{M}_1 & 0 & \bar{M}_3 \\ M_6 & 0 & M_4 & M_5 \\ 0 & \bar{M}_6 & \bar{M}_5 & \bar{M}_4 \end{pmatrix} \begin{pmatrix} z_1 \\ \bar{z}_1 \\ z_2 \\ \bar{z}_2 \end{pmatrix}, \quad (11)$$

where \bar{z}_1 denotes the complex conjugate of z_1 , *etc.*, and

$$\begin{aligned} M_1 &\equiv a_1 + ib_1 - i\omega + 2(c_1 + id_1)R_1^2 \\ M_2 &\equiv (c_1 + id_1)R_1^2 \\ M_3 &\equiv \gamma_1 \frac{R_2}{R_1} e^{i(\phi_2 - \phi_1 + \psi_1)} \\ M_4 &\equiv a_2 + ib_2 - i\omega + 2(c_2 + id_2)R_2^2 \\ M_5 &\equiv (c_2 + id_2)R_2^2 \\ M_6 &\equiv \gamma_2 \frac{R_1}{R_2} e^{i(\phi_1 - \phi_2 + \psi_2)}. \end{aligned} \quad (12)$$

The solution $A_j = R_j e^{i(\omega t + i\phi_j)}$, with R_j and ϕ_j satisfying (6)-(7), is stable if the eigenvalues of the matrix associated with the linearized problem (11) all have negative real part.

Figure 3(a) demonstrates the predicted transition from linear response to nonlinear response with $R_2 \propto F^{1/9}$. Figure 3(b) shows that as the damping in the system increases, larger forcings are necessary to reach this nonlinear regime. Moreover, this plot demonstrates the possibility of hysteresis which can occur when $b_j - \omega$ and d_j have opposite signs, provided the damping is not too great. Figure 3(c) shows how the transition from linear to $1/9$ scaling moves to larger forcing when the detuning $b_2 - \omega$ is increased; note that in this plot a scaling of $R_2 \propto F^{1/3}$ is also evident over an intermediate range of forcings. Changes in the magnitude of the feedback coefficient γ_1 can either enhance or degrade the response, R_2 , depending upon the coupling phases ψ_1 and ψ_2 . Figure 3(d) shows an example of the change in the response versus forcing relationship as the feedback coefficient, γ_1 , is increased.

B. Uniqueness and Stability: Unidirectional Coupling

The problem of determining the uniqueness and stability of solutions is greatly simplified in the case of unidirectional coupling between the mechanical and electrical resonators. In this section we focus our further analysis on the case where the feedback from the electrical resonator to the stereocilia can be neglected, *i.e.*, we focus on the case $\gamma_1 = 0$ in (4).

In this unidirectional-coupling case, $M_3 = 0$ in the stability matrix (11), and the linear stability problem simplifies to one of determining the eigenvalues associated with the 2×2 -blocks on the diagonal. For instance, if we let σ_1 and σ_2 be the eigenvalues associated with the $(\dot{z}_1, \dot{\bar{z}}_1)$ -equations, we find

$$\begin{aligned} \sigma_1 + \sigma_2 &= M_1 + \bar{M}_1 = 2(a_1 + 2c_1 R_1^2) \\ \sigma_1 \sigma_2 &= |M_1|^2 - |M_2|^2 = a_1^2 + (b_1 - \omega)^2 + 4[a_1 c_1 + (b_1 - \omega)d_1]R_1^2 + 3(c_1^2 + d_1^2)R_1^4. \end{aligned} \quad (13)$$

Similar equations for the remaining two eigenvalues, associated with the $(\dot{z}_2, \dot{\bar{z}}_2)$ -equations, hold: they are obtained from (13) by interchanging the 1 and 2 subscripts on its right-hand-side. In the case of supercritical Hopf bifurcations ($c_j < 0$), and damping of spontaneous oscillations ($a_j < 0$), the frequency-locked solutions are stable provided $|M_1|^2 - |M_2|^2 > 0$ and $|M_4|^2 - |M_5|^2 > 0$. While these conditions hold for sufficiently small and sufficiently large amplitudes R_1 and R_2 , they may be violated in the intermediate regime if $a_j c_j + (b_j - \omega)d_j < 0$ for either $j = 1$ or $j = 2$. Since we are interested in the case that a_j and c_j are both negative, a necessary condition for a frequency-locked solution to lose stability, with increase in forcing F , is that $b_j - \omega$ and d_j must have opposite signs. To gain some insight into this criterion, it is useful to note that the preferred frequencies, $b_1 + d_1 R_1^2$ and $b_2 + d_2 R_2^2$, of each tuning mechanism, in absence of forcing, are dependent upon response magnitude. If the natural frequency of the cell shifts away from the forcing frequency with increasing response ($[b_j - \omega]d_j > 0$), then $a_j c_j + (b_j - \omega)d_j > 0$ and the entrained solution is always stable and unique. Instabilities, and their associated hysteresis in the response *vs.* forcing curves, can only occur in the unidirectionally-coupled case if the preferred frequency of at least one of the tuning mechanisms

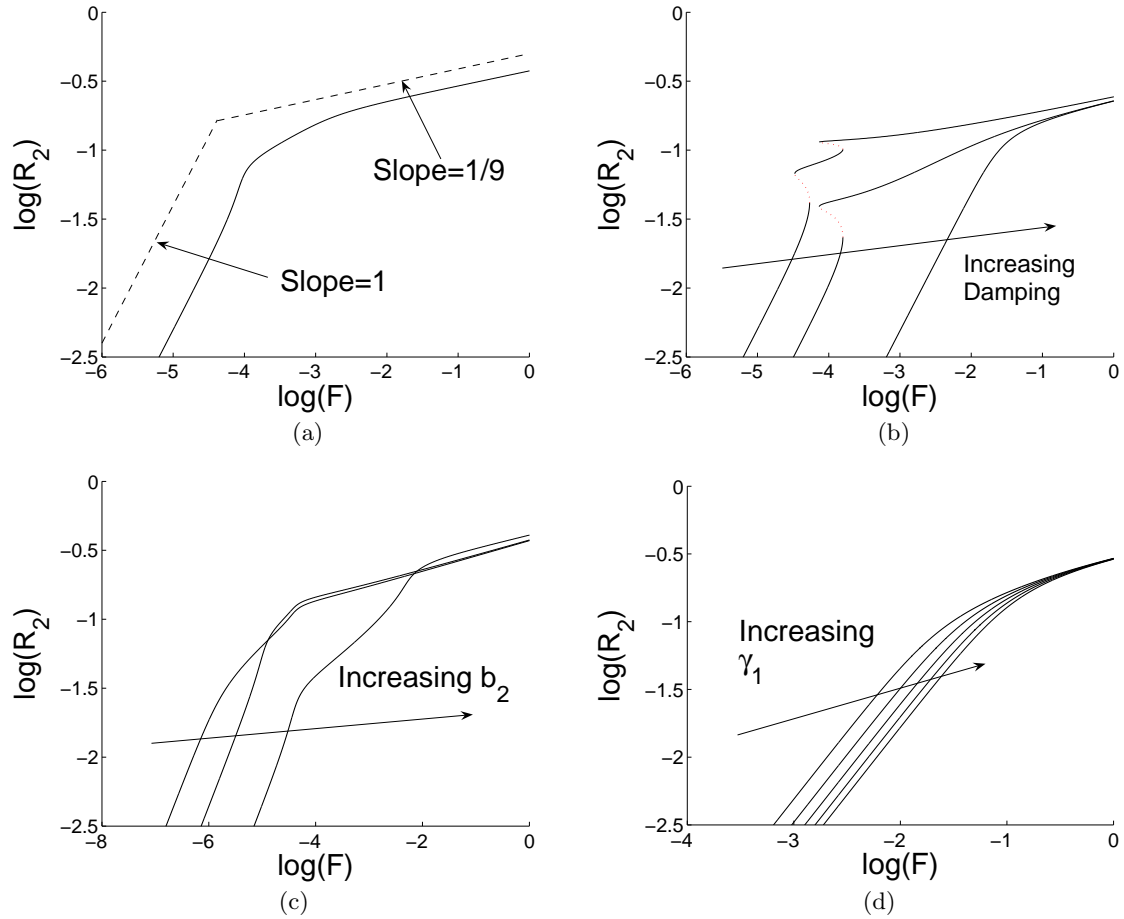


FIG. 3: Sample log-log plots of response (R_2) versus forcing (F) from (9-10), for the system with $c_1 = c_2 = -1$ and with varying damping, coupling, and detuning magnitudes. Solid (dotted) lines represent (un)stable frequency-locked solutions. (a) Transition from linear response ($R_2 \propto F$) to nonlinear response with $R \propto F^{1/9}$; dashed lines, for comparison, have slopes 1 and 1/9 as indicated. Parameters set to $a_1 = -0.02$, $a_2 = -0.001$, $b_1 - \omega = 0$, $b_2 - \omega = .01$, $d_1 = -2$, $d_2 = -1.1$, $\gamma_1 = 0$, $\gamma_2 = .1$, and $\psi_2 = 0.64\pi$. (b) Response curves obtained with linear damping parameters $(a_1, a_2) = (-.0002, -.0001), (-.0002, -.1), (-.2, -.1)$; other parameters set at $b_1 - \omega = .01$, $b_2 - \omega = .02$, $d_1 = -6$, $d_2 = -4$, $\gamma_1 = 0$, $\gamma_2 = .1$, and $\psi_2 = 0.64\pi$. (c) Response curves obtained with detuning $b_2 - \omega = .001, .01, .1$; other parameters set at $b_1 - \omega = .002$, $a_1 = -.001$, $a_2 = -.002$, $d_1 = -2$, $d_2 = -1.1$, $\gamma_1 = 0$, $\gamma_2 = .1$, and $\psi_2 = 0.64\pi$. (d) Response curves obtained with different backward coupling magnitudes of $\gamma_1 = 0, .1, .2, .3, .4$; other parameters set at $a_1 = -0.1$, $a_2 = -0.2$, $b_1 - \omega = 0.02$, $b_2 - \omega = 0.01$, $d_1 = -1$, $d_2 = -1.1$, $\gamma_2 = .1$, $\psi_1 = \pi$, $\psi_2 = 0$.

shifts towards the forcing frequency with increasing response amplitude ($(b_j - \omega)d_j < 0$). In this case, the system may jump from a small amplitude response to a larger amplitude one with an increase in the forcing. This follows from the observation that the instabilities, if they occur, come in pairs and correspond to saddle-node bifurcations along the solution branches $R_j(F)$; see Fig. 3(b) for examples. The necessary *and sufficient* condition for a pair of saddle-node bifurcations to occur is

$$a_j c_j + (b_j - \omega) d_j < -\sqrt{\frac{3}{4}(a_j^2 + (b_j - \omega)^2)(c_j^2 + d_j^2)}, \quad (14)$$

for $j = 1$ and/or $j = 2$. Note that the prediction that hysteresis can occur for larger detunings is a direct result of the dependence of the cell's preferred frequency on response amplitude, an effect which was neglected in previous studies for which the imaginary part of the nonlinear coefficient (d_j) was neglected [10, 11].

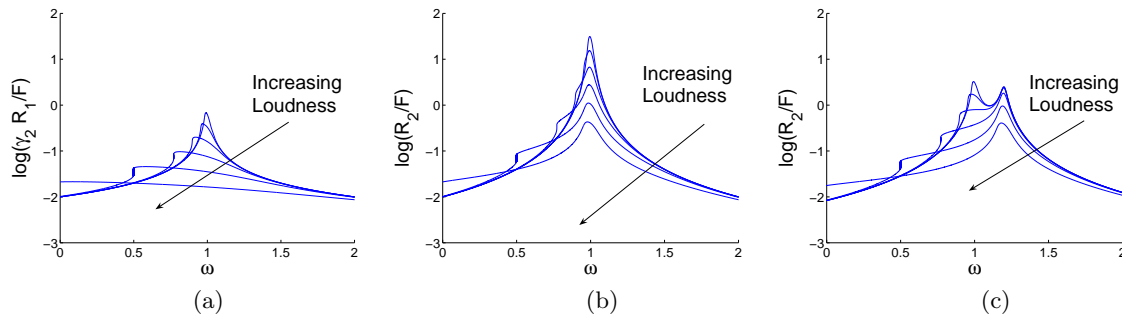


FIG. 4: Amplification *vs.* frequency plots from (8-9). Amplification was taken to be $\gamma_2 R_1/F$ in the single tuning mechanism case (a), and R_2/F in the double-tuning, uni-directionally coupled cases (b-c). Each curve represents a constant forcing amplitude taken from the set $F = 10^{-3}, 10^{-2.5}, 10^{-2.0} \dots 10^{-0.5}$ (a) $a_1 = -.01, b_1 = 1, c_1 = -1,$ and $d_1 = -2, \gamma_2 = .01, \psi_2 = 0.64\pi$. (b) $a_1 = -.01, a_2 = -.02, b_1 = b_2 = 1, c_1 = c_2 = -1, d_1 = -2, d_2 = -1.1, \gamma_1 = 0, \gamma_2 = 0.01, \psi_2 = 0.64\pi$. (c) $a_1 = -.01, a_2 = -.02, b_1 = 1, b_2 = 1.2, c_1 = c_2 = -1, d_1 = -2, d_2 = -1.1, \gamma_1 = 0, \gamma_2 = 0.01, \psi_2 = 0.64\pi$.

IV. RESULTS AND DISCUSSION

We expect that if each independent amplification mechanism is well-tuned to the forcing frequency ($|b_j - \omega| \ll 1$) and the damping is small the coupled system will have a greater response than a system with only a single tuning mechanism. From (10) we see that the leading coefficients α_j for $j = 1, \dots, 7$ in (9) may decrease in magnitude, compared to the highest order coefficient α_9 , as the forcing frequency ω approaches the natural frequencies of the tuning mechanisms, b_j . Figure 4 demonstrates that the amplification, $\frac{R_2}{F}$, is greatest near the resonant frequency. It also makes a comparison between the tuning curves for the coupled system and the system with one amplification mechanism suppressed. For the latter case we solve (6) for $R_1(\omega)$ with $R_2 = 0$, and then plot $\gamma_2 \frac{R_1}{F}$ as a function of frequency, for different values of F ; the coupling γ_2 is included so that the same relationship between the hair bundle displacement and the magnitude of the transduction current is assumed in both the single and the coupled tuning models. Each curve in the diagram shows the variation in response with forcing frequency, holding the signal amplitude F constant. Figure 4(a) shows that the broadest tuning curve occurs for the loudest sounds. As the magnitude of the sound decreases, several effects occur: the amplification increases, the frequency tuning becomes sharper, and because $d_j \neq 0$ the preferred frequency shifts as the magnitude of the forcing increases. We used $d_j < 0$ for all of the plots, so the preferred frequencies of the oscillation mechanisms decrease as their amplitude increases. This phenomenon in turn leads to a region of bistability for driving frequencies $\omega < b_j$ as described in Section III. This bistability is the source of the prominent shoulder in the tuning curves that appears for $\omega < 1$. A comparison of the height of the peaks in Figure 4(a) and (b), reveals that amplification of on-resonance forcing is enhanced in the coupled system. Also, the frequency tuning curves are sharper and display a smaller shift in frequency with changing forcing amplitude in the coupled system. Each of these properties would be a potential advantage of the coupled system. If the preferred frequencies of the two mechanisms are not sufficiently well-tuned to each other, then the single resonance peak in Fig. 4(b) may split into two peaks as seen in Fig. 4(c).

The algebraic relationship between the magnitude of the forcing and the magnitude of the response of the electrical resonance mechanism given in (9) allows for experimentally testable predictions to be made. In an idealized situation, for which each mechanism is perfectly tuned to the forcing frequency ($b_1 = b_2 = \omega$) and situated at the Hopf bifurcation ($a_1 = a_2 = 0$), equation (9) indicates that the response of the electrical resonance mechanism is proportional to $F^{\frac{1}{9}}$. The exponent, δ , of this response-versus-forcing relationship, $R_2 \propto F^\delta$, provides a measure of the quality of the amplification; small amplitude signals are amplified to a greater extent for smaller values of δ . For a system employing only a single tuning mechanism, critically tuned to the bifurcation point and forcing frequency, the expected scaling is $R \propto F^{\frac{1}{3}}$ [10, 11]. The smaller exponent of $\delta = 1/9$, associated with the well-tuned coupled model, can provide more powerful amplification (R_2/F) than a system with an isolated tuning mechanism. In more realistic situations for which some damping and/or detuning is present ($a_j < 0, b_j \neq \omega$), equation (9) predicts a transition from a regime in which $R_2 \propto F$ for smaller forcings and a regime in which $R_2 \propto F^{1/9}$ for sufficiently large signals. By measuring the response of the electrical resonance mechanism for different amplitudes of signal, it is possible to estimate δ , although, depending upon which portion of the response-versus-forcing curve is sampled, different estimates for δ might be obtained experimentally.

In comparing the scaling predictions of our model to experiment, we turn to auditory nerve data. Changes in the membrane potential of the hair cell body result in the release of neurotransmitters at the hair cell-auditory nerve synapse. Larger depolarizations result in larger amounts of neurotransmitter release and thus a faster firing rate in

the auditory nerve. There is biological evidence that, even for nonresonant stimuli, the firing rate at the auditory nerve is a nonlinear function of the sound stimulus. However, this nonlinearity, which occurs either due to synaptic effects or the relationship between hair bundle displacement and DC receptor potential, is factored out during the data analysis, allowing an estimate of δ to be made (see discussion in [25, 26]).

Numerous experiments have been performed in order to estimate the exponent, δ , of the response-versus-forcing relationship from experimental auditory nerve recordings. Table I summarizes some recent measurements of δ taken from experiments in both mammals and nonmammals. In each case, δ is commonly measured to be smaller than $1/3$. In mammals, as in nonmammals, two different mechanisms have been proposed to explain amplification, the first due to active motion of outer hair cells [27, 28], and the second due to the active motion of the hair bundles [6, 29, 30, 31]. While our results do not directly apply to mammalian data, as the coupling of the two active elements may be more complicated [32], it is noteworthy that compression estimates in mammals are similar to those in nonmammals.

Table I. Experimental estimates of δ
Nonmammals:
Owls: between 0.05 and 0.55, with the majority of data points lying between 0.1 and 0.3 [33]
Pigeons: between 0.22 and 0.6 [34]
Mammals:
Guinea-pigs: between 0.2 and 0.25 [25].
Guinea-pigs: approximately 0.6 for two low- frequency (1.8 and 2.7 kHz.) fibers, and approximately 0.1 for medium- (5.5-6.3 kHz) and high-frequency (20.5-23 kHz) fibers. For fibers tuned above 4 kHz, the mean exponent was 0.13 with a standard deviation of 0.04 [35].
Chinchilla: direct basilar membrane measurements yield δ values between 0.2 and 0.7 [36].

The observation of δ values smaller than $1/3$ is interesting in that it indicates that the auditory system achieves greater compressions than would be expected from a system with a single tuning mechanism associated with a Hopf bifurcation. Experimental measurements of the forcing-versus-displacement relationship for individual hair bundles satisfy the $R \propto F^{1/3}$ scaling law expected for a system tuned near a generic Hopf bifurcation [10, 11]. Because effects at the synapse are removed during the data analysis, any additional compression must occur due to the interaction with the electrical resonance mechanism.

Some models have explained this increased compression by assuming within their model, that the leading nonlinear terms are higher than cubic (e.g.[37]). We propose that a more physically motivated way of achieving higher order compression would be through the coupling of two systems tuned near a Hopf bifurcation. With the exception of three data points, all δ -values in Köppl and Yates' owl data are greater than .1, with the majority of measurements lying between .1 and .3 [37]. So their data is not inconsistent with what would be expected from a coupled system, which at best produces a δ -value of $1/9$. If it is the case that the observed enhanced amplification occurs due to coupling between the two tuning mechanisms, this is an interesting result, because our analysis indicates that the tuning mechanisms must maintain themselves close to the bifurcation point and close to the same frequency for maximum amplification to be observed. It would be interesting both from a biological and mathematical perspective to understand how such fine tuning is achieved. Some studies have suggested that stochastic effects may help the system adjust itself to the bifurcation point [38, 39]. Another has suggested that with certain assumptions about the evolution of the bifurcation parameter, self-tuning occurs automatically [40]. Biologically, it has been suggested that adjustments in the tension of the hair bundle due to an actin myosin mechanism may act to keep the hair bundle properly tuned [24, 41].

Another prediction of the model is that the response of the electrical resonance mechanism may be hysteretic for sufficiently large frequency detuning. It is worth noting that this feature arises as a direct result of shift in the natural frequency of the tuning mechanisms with increasing response, a feature that was not taken into account in previous models. It would be interesting if such bistability could be observed in experimental auditory nerve data.

Acknowledgments

K.A.M. is grateful for fellowship support through NSF-IGERT grant DGE-9987577 and NSF-RTG grant 0354259. M.S. acknowledges support through NSF Grant DMS-0309667.

V. APPENDIX I

Model Proposed by Hudspeth and Lewis

The following seven-dimensional model of a bullfrog saccular hair cell was proposed by Hudspeth and Lewis [12, 13]. It is a Hodgkin and Huxley type model with three ion channels included in the model, a voltage-gated calcium ion channel, a calcium-gated potassium ion channel, and a passive leakage channel. The passive leakage channel is always open. The calcium ion channel opens in response to depolarization. The gating of the potassium ion channel requires both the binding of calcium to the interior of the channel and an adequate depolarization. The first equation models the rate of change of the membrane potential (V_m) due to currents entering the cell through both the transduction channels, the calcium ion channels, and the calcium-gated potassium channels. The other six equations account for changes in the concentration of internal calcium (Ca) close to the membrane, the fraction of open calcium ion channels (m), and the fraction of potassium ion channels in each of three closed configurations (C_0, C_1, C_2) and two open configurations (O_2, O_3).

$$\begin{aligned}
C_m \frac{dV_m}{dt} &= -g_{Ca} m^3 (V_m - E_{Ca}) \\
&\quad -g_{K(Ca)} (O_2 + O_3) (V_m - E_K) \\
&\quad -g_L (V_m - E_L) + I \\
\frac{dCa}{dt} &= -\frac{U g_{Ca} m^3 (V_m - E_{Ca})}{z F v_{cell} \xi} - K_s Ca \\
\frac{dm}{dt} &= \beta(V_m) (1 - m) - \alpha(V_m) m \\
\frac{dC_0}{dt} &= k_{-1} C_1 - k_1 Ca C_0 \\
\frac{dC_1}{dt} &= k_1 Ca C_0 + k_{-2} C_2 - (k_{-1} + k_2 Ca) C_1 \\
\frac{dC_2}{dt} &= k_2 Ca C_1 + \alpha_{C_0} e^{-V_m/V_{aa}} O_2 - (k_{-2} + \beta_C) C_2 \\
\frac{dO_2}{dt} &= \beta_C C_2 + k_{-3} O_3 - (\alpha_{C_0} e^{-V_m/V_{aa}} + k_3 Ca) O_2 \\
O_3 &= 1 - C_0 - C_1 - C_2 - O_2
\end{aligned} \tag{15}$$

where

$$\begin{aligned}
\alpha(V_m) &= \alpha_0 e^{-(V_m + V_0)/V_A} + K_A \\
\beta(V_m) &= \beta_0 e^{(V_m + V_0)/V_B} + K_B \\
k_1 &= \frac{k_{-1}}{K_{10} e^{\frac{\delta_1 z F V_m}{RT}}} \\
k_2 &= \frac{k_{-2}}{K_{20} e^{\frac{\delta_2 z F V_m}{RT}}} \\
k_3 &= \frac{k_{-3}}{K_{30} e^{\frac{\delta_3 z F V_m}{RT}}}
\end{aligned}$$

The amount of current that is injected into the cell, I , is used as the control parameter. All other parameters are set to the value used in Hudspeth and Lewis's original paper: $g_{Ca} = 4.14 \times 10^{-9}$ S, $E_{Ca} = .1$ V, $g_{K_{Ca}} = 16.8 \times 10^{-9}$ S, $E_K = -.08$ V, $E_L = -.03$ V, $g_L = 10^{-9}$ S, $C_m = 15 \times 10^{-12}$ F, $U = .02, z = 2, F = 96485.309$ C/mol, $v_{cell} = 1.25 \times 10^{-12}$ L, $\xi = 3.4 \times 10^{-5}$, $K_s = 2800$ s $^{-1}$, $\beta_0 = .97$ s $^{-1}$, $V_0 = .07$ V, $V_B = .00617$ V, $K_B = 940$ s $^{-1}$, $K_A = 510$ s $^{-1}$, $V_A = .00801$ V, $\alpha_0 = 22800$ s $^{-1}$, $\alpha_{C_0} = 450$ s $^{-1}$, $T = 295$ K, $R = 8.314510$ $\frac{J}{mol \cdot K}$, $\delta_1 = .2, \delta_2 = 0, \delta_3 = .2, \beta_C = 1000$ s $^{-1}$, $k_{-1} = 300$ s $^{-1}$, $k_{-2} = 5000$ s $^{-1}$, $k_{-3} = 1500$ s $^{-1}$, $K_{10} = 6 \times 10^{-6}$ M, $K_{20} = 45 \times 10^{-6}$ M, $K_{30} = 20 \times 10^{-6}$ M, and $V_{aa} = .033$ V.

VI. APPENDIX II

Here we present some details of the reduction of the Hudspeth and Lewis model (15) to the normal form (3). Our analysis is valid in a neighborhood of the equilibrium solution ($V_m^*, Ca^*, m^*, C_0^*, C_1^*, C_2^*, O_2^*$) for command currents

I sufficiently close to the critical current I^* . In particular, we find that $V_m^* \approx -0.04888$ V, $Ca^* \approx 1.623 \times 10^{-5}$, $m^* \approx 0.3115$, $C_0^* \approx 0.08429$, $C_1^* \approx 0.4919$, $C_2^* \approx 0.1774$, $O_2^* \approx 0.08960$, and $O_3^* \approx 0.1568$, for $I = I^* \approx 91.3 \times 10^{-12}$ A.

We first translate the fixed point to the origin and nondimensionalize variables as follows: $V_m = V_m^*(1 + X_1)$, $Ca = Ca^*(1 + X_2)$, $m = m^*(1 + X_3)$, $C_0 = C_0^*(1 + X_4)$, $C_1 = C_1^*(1 + X_5)$, $C_2 = C_2^*(1 + X_6)$, $O_2 = O_2^*(1 + X_7)$. Moreover, we let $I = I^*(1 + \Delta I)$, where ΔI measures a small deviation from the critical command current associated with the Hopf bifurcation, and allow for a small periodic forcing through the leakage current conductance by setting $g_L = g_L^*(1 + \Delta g_L(t))$. Here $\Delta g_L(t) = \Delta g_L(t + T)$ captures the purely oscillatory part of g_L , while g_L^* is the mean conductance; we set $g_L^* = 10^{-9}$ S, as in the original Hudspeth and Lewis model. The period T is related to the forcing frequency ω in the usual fashion, $T \equiv 2\pi/\omega$. The governing equations, expressed in terms of the dimensionless vector-valued variable $\mathbf{X} = (X_1, X_2, \dots, X_7)$ and the parameters ΔI and $\Delta g_L(t)$, are written

$$\frac{d\mathbf{X}}{dt} = \mathbf{H}(\mathbf{X}; \Delta I, \Delta g_L(t)) . \quad (16)$$

The Hopf bifurcation occurs at $\mathbf{X} = \mathbf{0}$, $\Delta I = 0$ for $\Delta g_L(t) = 0$, so $\mathbf{H}(\mathbf{0}; 0, 0) = \mathbf{0}$ and the Jacobian matrix $\mathbf{DH}(\mathbf{0}; 0, 0)$ has a pair of purely imaginary eigenvalues $\pm i\omega_0$, $\omega_0 \approx 938$ s $^{-1}$, with associated complex eigenvectors $\mathbf{U}, \overline{\mathbf{U}}$. The remaining eigenvalues $\lambda_1, \dots, \lambda_5$ (where $\lambda_5 = \overline{\lambda_4}$) all have real parts less than -2000 s $^{-1}$ (see Fig. 2), and are associated with eigenvectors $\mathbf{V}_1, \dots, \mathbf{V}_5$ (where, again, $\mathbf{V}_5 = \overline{\mathbf{V}_4}$). Our convention is to normalize all eigenvectors to 1. Finally, we diagonalize the linearized problem at the bifurcation point by letting $\mathbf{X}(t) = z(t)\mathbf{U} + \overline{z}(t)\overline{\mathbf{U}} + y_1(t)\mathbf{V}_1 + y_2(t)\mathbf{V}_2 + \dots + y_5(t)\mathbf{V}_5$, and write the governing equations in terms of the new variables $z, \overline{z}, \mathbf{y} \equiv (y_1, \dots, y_5)$ as follows:

$$\begin{aligned} \frac{dz}{dt} &= i\omega_0 z + N_z(z, \overline{z}, \mathbf{y}; \Delta I, \Delta g_L(t)), \\ \frac{d\overline{z}}{dt} &= -i\omega_0 \overline{z} + \overline{N}_z(z, \overline{z}, \mathbf{y}; \Delta I, \Delta g_L(t)), \\ \frac{d\mathbf{y}}{dt} &= \Lambda \mathbf{y} + \mathbf{N}_y(z, \overline{z}, \mathbf{y}; \Delta I, \Delta g_L(t)) . \end{aligned} \quad (17)$$

Here Λ is a diagonal matrix, with eigenvalues $\lambda_1, \dots, \lambda_5$ on the diagonal, and N_z and \mathbf{N}_y contain the nonlinear terms in z, \overline{z} and \mathbf{y} , as well as all terms involving the parameters ΔI and $\Delta g_L(t)$.

We now use perturbation theory to derive the normal form of the bifurcation problem. Toward this end we introduce a small book-keeping parameter ϵ ($|\epsilon| \ll 1$) that is a measure of proximity to the Hopf bifurcation. Specifically, we let $\Delta I = \epsilon^2 \mu$ and seek small amplitude solutions of the form

$$\begin{aligned} z(t) &= \epsilon z_1(t, T) + \epsilon^2 z_2(t, T) + \epsilon^3 z_3(t, T) + \dots , \\ \mathbf{y}(t) &= \epsilon^2 \mathbf{y}_2(t, T) + \epsilon^3 \mathbf{y}_3(t, T) + \dots , \end{aligned} \quad (18)$$

where $T = \epsilon^2 t$ is a slow time variable that captures the slow decay to the oscillatory solutions associated with a Hopf bifurcation. Finally, we make some additional assumptions about the magnitude and frequency of the applied periodic forcing by letting $\Delta g_L(t) = \epsilon^3 f(t)$ and $\omega_0 = \omega + \epsilon^2 \hat{\omega}$, *i.e.* we consider small nearly-resonant periodic forcing.

Inserting these ansatz in equation (17), and expanding in powers of ϵ , we recover at $\mathcal{O}(\epsilon)$

$$\frac{\partial z_1}{\partial t} = i\omega z_1, \quad (19)$$

with solution

$$z_1 = \hat{A}(T) e^{i\omega t} . \quad (20)$$

Here the complex amplitude $\hat{A}(T)$ satisfies an equation to be determined at higher order.

At $\mathcal{O}(\epsilon^2)$, we find

$$\frac{\partial z_2}{\partial t} = i\omega z_2 + \alpha_z \mu + \beta_z z_1^2 + \gamma_z \overline{z}_1^2 + \delta_z |z_1|^2, \quad (21)$$

where $\alpha_z \approx -756 + 52i$, $\beta_z \approx -86 + 2i$, $\gamma_z \approx 20 - 20i$, $\delta_z \approx -80 - 64i$, as well as similar equations for the fast-time evolution of \mathbf{y}_2 . The general solution of (21) is

$$z_2(t, T) = \frac{i(\alpha_z \mu + \delta_z |\hat{A}|^2)}{\omega} - \frac{i\beta_z \hat{A}^2}{\omega} e^{2i\omega t} + \frac{i\gamma_z \overline{\hat{A}}^2}{3\omega} e^{-2i\omega t} + \hat{B}(T) e^{i\omega t} . \quad (22)$$

Here $\hat{B}(T)$ is arbitrary and we set it to zero in the remainder of our computations, since, without loss of generality, it may be absorbed by the $\mathcal{O}(\epsilon)$ solution (20). The equations for each of the components of \mathbf{y}_2 , which have a similar structure to (21), yield solutions of the same form as (22), although with $\hat{B}(T)e^{i\omega t}$ replaced by rapidly decaying solutions $C_j(T)e^{\lambda_j t}$ of their associated homogeneous problems.

Finally, at $\mathcal{O}(\epsilon^3)$, we find

$$\frac{\partial z_3}{\partial t} = i\omega z_3 + \left(i\hat{\omega}\hat{A} - \frac{\partial \hat{A}}{\partial T} + (45 + 97i)\mu\hat{A} - (46 + 49i)|\hat{A}|^2\hat{A} - (156 - 11i)\hat{f}_1 \right) e^{i\omega t} + \dots \quad (23)$$

Here the ellipsis indicates additional terms proportional to $e^{-i\omega t}$ and $e^{\pm 3i\omega t}$, and \hat{f}_1 is the coefficient of the $e^{i\omega t}$ term in the Fourier expansion of the periodic forcing function $f(t)$. We have written explicitly only those terms on the right-hand-side that are resonant with the solution of the linear homogeneous problem. In order for our perturbation expansion to remain valid, this resonant forcing term, which leads to unbounded growth, must vanish. In this fashion we obtain the following evolution equation for $\hat{A}(T)$:

$$\frac{\partial \hat{A}}{\partial T} = i\hat{\omega}\hat{A} + (45 + 97i)\mu\hat{A} - (46 + 49i)|\hat{A}|^2\hat{A} - (156 - 11i)\hat{f}_1. \quad (24)$$

Finally, we re-write the equation in the normal form (3) by letting

$$A(t) = \epsilon\hat{A}(\epsilon^2 t)e^{i\omega t + i\varphi}, \quad (25)$$

where the phase φ is specified below. We then find

$$\frac{dA}{dt} = (a + ib)A + (c + id)|A|^2A + Fe^{i\omega t}, \quad (26)$$

where

$$\begin{aligned} a + ib &= 45\Delta I + i(\omega_0 + 97\Delta I), \\ c + id &= -(46 + 49i), \\ F &= -(156 - 11i)\widehat{\Delta g}_{L,1}e^{i\varphi}. \end{aligned} \quad (27)$$

Here $\widehat{\Delta g}_{L,1}$ is the coefficient of the $e^{i\omega t}$ term in the Fourier expansion of Δg_L , and we choose φ so that F is real and positive, *i.e.* so that

$$F = |(156 - 11i)\widehat{\Delta g}_{L,1}|. \quad (28)$$

Next, we will consider how two systems tuned near a Hopf bifurcation would interact. Under the assumption that the coupling between the two systems is weak and linear, it's straightforward to show that the coupled system can be described by the following set of coupled amplitude equations.

$$\frac{dA_1}{dt} = (a_1 + b_1i)A_1 + (c_1 + d_1i)|A_1|^2A_1 + \gamma_1e^{i\psi_1}A_2 + Fe^{i\omega t}, \quad (29)$$

$$\frac{dA_2}{dt} = (a_2 + b_2i)A_2 + (c_2 + d_2i)|A_2|^2A_2 + \gamma_2e^{i\psi_2}A_1, \quad (30)$$

where the coefficients of the coupling terms, γ_1 and γ_2 , are taken to be of order ϵ^2 indicating weak coupling between the two systems. Additionally, for coupling between the two systems to occur, it is necessary to assume that the resonance frequency of each system is within ϵ^2 of the forcing frequency ω . As with the previous amplitude equations, the resonant forcing amplitude, F , is assumed to be small on the order of ϵ^3 and each system is assumed to be tuned sufficiently close to the Hopf bifurcation, requiring that both a_1 and a_2 be of order ϵ^2 .

[1] L. Robles and M. A. Ruggero, *Physiol. Rev.* **81**(3), 1305 (2001).

- [2] G. A. Manley, *J. Neurophysiol.* **86**(2), 541 (2001).
- [3] R. Fettdiplace, A. J. Ricci, and C. M. Hackney, *Trends in Neurosciences* **24**(3), 169 (2001).
- [4] E. R. Kandel, J. H. Schwartz, and T. M. Jessell, *Principles of Neural Science, Fourth Edition* (McGraw-Hill, New York, 2000).
- [5] A. J. Hudspeth, *Nature* **341**(6241), 397 (1989).
- [6] P. Martin and A. J. Hudspeth, *P. Natl. Acad. Sci.* **96**(25), 14306 (1999).
- [7] R. Fettdiplace and A. C. Crawford, *P. Roy. Soc. Lond. B* **203**, 209 (1978).
- [8] Y. Choe, M. O. Magnasco, and A. J. Hudspeth, *P. Natl. Acad. Sci.* **95**(26), 15321 (1998).
- [9] M. Ospeck, V. M. Eguíluz, and M. O. Magnasco, *Biophys. J.* **80**(6), 2597 (2001).
- [10] V. M. Eguíluz, M. Ospeck, Y. Choe, A. J. Hudspeth, and M. O. Magnasco, *Phys. Rev. Lett.* **84**(22), 5232 (2000).
- [11] S. Camalet, T. Duke, F. Jülicher, and J. Prost, *P. Natl. Acad. Sci.* **97**(7), 3183 (2000).
- [12] A. J. Hudspeth and R. S. Lewis, *J. Physiol. (Lond.)* **400**, 237 (1988).
- [13] A. J. Hudspeth and R. S. Lewis, *J. Physiol. (Lond.)* **400**, 275 (1988).
- [14] S. Wiggins, *Introduction to Applied Nonlinear Dynamical Systems and Chaos*, vol. 2 of *Texts in Applied Mathematics* (Springer-Verlag, New York, 1990).
- [15] E. L. M. Cheung and D. P. Corey, *Biophys. J.* **90**, 124 (2006).
- [16] P. Martin and A. J. Hudspeth, *P. Natl. Acad. Sci.* **98**(25), 14386 (2001).
- [17] A. J. Hudspeth and D. P. Corey, *P. Natl. Acad. Sci.* **74**(6), 2407 (1977).
- [18] J. A. Assad and D. P. Corey, *J. Neurosci.* **12**(9), 3291 (1992).
- [19] W. Denk and W. W. Webb, *Hearing Res.* **60**(1), 89 (1992).
- [20] A. J. Ricci, A. C. Crawford, and R. Fettdiplace, *J. Neurosci.* **20**(19), 7131 (2000).
- [21] A. J. Ricci, A. C. Crawford, and R. Fettdiplace, *J. Neurosci.* **22**(1), 44 (2002).
- [22] D. Bozovic and A. J. Hudspeth, *P. Natl. Acad. Sci.* **100**(3), 958 (2003).
- [23] A. Rüschi and U. Thurm, *Hearing Res.* **48**(3), 247 (1990).
- [24] P. Martin, D. Bozovic, Y. Choe, and A. J. Hudspeth, *J. Neurosci.* **23**(11), 4533 (2003).
- [25] G. K. Yates, I. M. Winter, and D. Robertson, *Hearing Res.* **45**(3), 203 (1990).
- [26] G. K. Yates, G. A. Manley, and C. Köppl, *J. Acoust. Soc. Am.* **107**(4), 2143 (2000).
- [27] J. F. Ashmore, *J. Physiol. (Lond.)* **388**, 323 (1987).
- [28] J. Santos-Sacchi and J. P. Dilger, *Hearing Res.* **35**(2-3), 143 (1988).
- [29] A. C. Crawford and R. Fettdiplace, *J. Physiol. (Lond.)* **364**, 359 (1985).
- [30] M. E. Benser, R. E. Marquis, and A. J. Hudspeth, *J. Neurosci.* **16**(18), 5629 (1996).
- [31] H. J. Kennedy, A. C. Crawford, and R. Fettdiplace, *Nature* **433**, 880 (2005).
- [32] H. J. Kennedy, M. G. Evans, A. C. Crawford, and R. Fettdiplace, *J. Neurosci.* **26**(10), 2757 (2006).
- [33] C. Köppl and G. Yates, *J. Neurosci.* **19**(21), 9674 (1999).
- [34] C.-P. Richter, S. Heynert, and R. Klinke, *Hearing Res.* **83**(1-2), 19 (1995).
- [35] N. P. Cooper and G. K. Yates, *Hearing Res.* **78** (2), 221 (1994).
- [36] M. A. Ruggero, N. C. Rich, A. Recio, S. S. Narayan, and L. Robles, *J. Acoust. Soc. Am.* **101**(4), 2151 (1997).
- [37] G. K. Yates, *Hearing Res.* **50**(1-2), 145 (1990).
- [38] B. Nadrowski, P. Martin, and F. Jülicher, *P. Natl. Acad. Sci.* **101**(33), 12195 (2004).
- [39] J. Balakrishnan, *J. Phys. A: Math. Gen.* **38**, 1627 (2005).
- [40] L. Moreau and E. Sontag, *Phys. Rev. E* **68**, 020901 (2003).
- [41] A. Vilfan and T. Duke, *Biophys. J.* **85**, 191 (2003).